IEEE Access
Multidisciplinary ⋮ Rapid Review ⋮ Open Access Journal

Received 24 October 2023, accepted 8 November 2023, date of publication 23 November 2023,
date of current version 1 December 2023.

Digital Object Identifier 10.1109/ACCESS.2023.3335992

RESEARCH ARTICLE

Explicit Model Predictive Speed Control for Permanent Magnet Synchronous Motor With Torque Ripple Minimization

TY TRUNG NGUYEN, TON HOANG NGUYEN, AND JAE WOOK JEON, (Senior Member, IEEE)
Department of Electrical and Computer Engineering, Sungkyunkwan University, Suwon 16419, South Korea

Corresponding author: Jae Wook Jeon (jwjeon@skku.edu)

This work was supported by Institute of Information and Communications Technology Planning and Evaluation (IITP) grant funded by the Korea government [MSIT(Ministry of Science and Information and Communication Technology)] (2021-0-01364, An intelligent system for 24/7 real-time traffic surveillance on edge devices).

ABSTRACT Permanent Magnet Synchronous Motors (PMSMs) are employed in various high-precision industrial applications. However, the torque ripple caused by nonideal factors, such as cogging torque, flux harmonics, and unbalanced stator phase currents diminishes motor performance. Therefore, torque ripple minimization is an important key in designing high-performance controllers for PMSMs. In this paper, an explicit model predictive speed control (EMPSC) is proposed as an advanced strategy for torque ripple minimization. First, the torque ripple is modeled as a periodic disturbance in the speed model. Subsequently, a Lyapunov-based periodic disturbance observer (PDOB) is designed to fast and accurately estimate the torque ripple. The EMPSC updates the estimated disturbance into the prediction model and minimizes the cost function to obtain the optimal control signal. This control signal effectively mitigates torque ripple while enhancing dynamic response performance. Furthermore, this paper introduces an explicit process aimed at significantly reducing the complexity and computational effort of the entire control scheme. Lastly, the simulation and experimental results are presented to demonstrate the effectiveness of the proposed method.

INDEX TERMS Torque ripple minimization, periodic disturbance observer, explicit model predictive control, permanent magnet synchronous motor (PMSM).

I. INTRODUCTION

Over the past few decades, permanent magnet synchronous motors (PMSMs) have been widely applied in various motion control applications, especially in high-precision fields such as industrial robots, medical instruments, and automotive systems, due to the advantages of a high torque-to-inertia ratio, high power density, and high efficiency [1].

However, the existence of parasitic torque ripple remains a significant disadvantage in PMSM drives. The torque ripple can generate periodic speed oscillations, especially in the low-speed range, thereby degrading the speed-tracking performance. Additionally, periodic speed oscillation also causes mechanical vibrations and reduces the lifetime of the motor system.

Generally, the torque ripple in PMSM is usually caused by two main sources. The first source arises from the motor structure, which includes cogging torque and flux harmonics. The second source comes from the drive controller, such as dead time effect, unbalanced stator phase, and current measurement errors. Over the past two decades, researchers have proposed various techniques for minimizing torque ripple, which can be categorized into two approaches. The first approach aims to optimize and develop the motor structure to eliminate torque ripple parasitism. In [2], [3], and [4], several advanced motor structure designs are proposed, such as improvements in winding distribution and skewing of stator lamination slots. These design innovations can achieve good control performance with a significant

The associate editor coordinating the review of this manuscript and approving it for publication was Feifei Bu.

reduction in torque ripple. However, these enhanced structures require special designs and involve a complex manufacturing process. As a result, the cost of the motor increases.

The second approach, presented in [5], [6], [7], [8], [9], [10], [11], and [12], focuses on designing advanced control techniques to mitigate the influence of torque ripple. In [5], a Lagrange multiplier-based method is introduced to calculate the optimal stator current that minimizes torque ripple. Additionally, a genetic algorithm [6] and an artificial neural network-based method [7] are also presented to determine the optimal current control signal that minimizes torque ripple. The results obtained in [6] and [7] illustrate the effectiveness of torque ripple minimization. However, these methods have disadvantages in terms of computational burden and complex implementation. In [8] and [9], various proportional-integral resonant (PIR) control strategies have been proposed to reduce torque ripple by mitigating periodic disturbances, including back EMF harmonics and dead time effect in the current loop, as well as cogging torque and current measurement errors in the speed loop. However, the resonant term is designed for a particular perturbation frequency. Consequently, when facing significant frequency disturbances, the effectiveness of PIR control in minimizing torque ripple may be compromised. A fuzzy logic control has been proposed in [10] to address the torque ripple of PMSM in the presence of parameter mismatches. However, the effectiveness of these fuzzy controllers depends on expert knowledge and an extensive tuning process to achieve effective torque ripple minimization performance. In [11] and [12], iterative learning control (ILC) techniques have also been proposed to mitigate torque ripple by compensating for periodic disturbances. However, a drawback of the ILC method is its sensitivity to system uncertainties and variations.

In recent years, model predictive control (MPC) has attracted much research attention due to its fast dynamic performance and ability to handle constraints [13], [14], [15], [16], [17], [18], [19]. For motor systems, numerous control algorithms based on MPC have been proposed to reduce the torque ripple of PMSM, such as quantized searching [20] and duty-cycle control [21], [22], [23]. In [24], a cascade MPC control structure with a sinusoidal disturbance compensator is proposed to reduce the torque ripple caused by the current sensor offset errors. However, the torque ripple model in [24] addresses a specific source of torque ripple, whereas in PMSMs, torque ripple is generally caused by multiple sources concurrently. Moreover, the load torque disturbance is not considered. In [25] the MPC combined with repetitive control (RC) is introduced to reduce the influence of both parameter mismatches and torque ripple. However, similar to PIR-based methods, repetitive control becomes complex when dealing with multiple frequency disturbances. In [26], an FCS-MPC scheme with a state observer and a feed-forward compensating signal is designed to minimize the torque oscillations produced by the nonsinusoidal flux linkage. However, as mentioned in [24], the FCS-MPC requires a variable sampling frequency and possibly leads to current ripples. In [27] and [28], the combination of an MPC with an ILC has been introduced to estimate and suppress the periodic velocity pulsation caused by the torque ripple. However, the iteration process of ILC in this method is complex and time-consuming.

However, none of the aforementioned MPC-based control methods have considered the complexity and computational volume. In general, the implementation of MPC requires solving online optimization during each sampling instant. However, solving online optimization by using the iterative computation algorithm, such as the active-set method or interior-point method is usually computationally complex and time-consuming. This is also an obstacle of MPC when practically applied in fast dynamic systems, such as power systems and electric machines. To overcome this drawback, an explicit approach was introduced in [30] for constrained MPC. In explicit MPC, the optimization problem can be pre-solved in the offline stage, and the optimal control law is formulated as a piecewise affine (PWA) function. As a result, explicit MPC can significantly reduce the computational load and is suitable for real-time implementation of MPC. Several explicit MPC methodologies [31], [32], [33] have been effectively employed in position, speed, and current control of PMSM.

Given the aforementioned problems, this paper proposes a simple technique for minimizing torque ripple using the explicit model predictive speed control (EMPSC) combined with a periodic disturbance observer (PDOB). The major advantages of the proposed control strategy are summarized as follows:

1) The PDOB is presented for online estimation of the periodic disturbance components in the speed model which generate the torque ripple. Compared to the existing observers, the proposed PDOB can handle a wide range of harmonic and is easy to implement.
2) The design of EMPSC with a modified cost function is proposed to calculate the optimal control signal. This optimal control signal achieves fast dynamic response, robustness against disturbances, and effective torque ripple minimization.
3) Significant reduction in computational complexity compared to conventional MPC-based methods.

The remainder of this paper is organized as follows. In Section II, the mathematical model of the PMSM and the influence of torque ripple are described. In Section III, the design of the PDOB for online estimation of torque ripple disturbance is introduced. Section IV presents the design of the EMPC. The explicit process for online solving the optimization problem is also introduced in this section. The simulation study and experimental results are discussed in Section V and Section VI. Finally, the conclusions of this paper are summarized in Section VII.

II. MATHEMATICAL MODEL OF PMSM

The stator current equations of the PMSM in the $d-q$ frame can be described as follows:

$$\begin{cases} L_d \dfrac{di_d}{dt} = u_d - R_s i_d + \omega_e L_q i_q \\ L_q \dfrac{di_q}{dt} = u_q - R_s i_q - \omega_e L_d i_d - \omega_e \psi_f \end{cases} \tag{1}$$

where i_d, i_q, u_d, u_q are the stator current and voltage along the d- q axis, respectively; R_s denotes the stator windings per-phase resistance, ψ_f is the flux linkage of the permanent magnet, L_q, L_d present the stator winding inductances in the q axis and d axis, respectively; and ω_e is the rotor electrical speed. Here $\omega_e = p\omega$ where ω is the rotor mechanical speed and p is the number of pole pairs. The dynamic model of the PMSM can be expressed as follows:

$$J\frac{d\omega}{dt} + F\omega + T_L = T_m \tag{2}$$

where J and F present the moment of total inertia and the viscous coefficient, respectively; T_L is the load torque and T_m is the motor generated torque. Generally, the motor torque consists of the electromagnetic torque T_E and the parasitic torque pulsation T_R. The torque T_E is produced by the interaction of the time-varying stator voltage and the permanent magnet rotor field.

$$T_E = \frac{3}{2}p\big(\psi_f i_q - (L_q - L_d) i_d i_q\big) \tag{3}$$

For the surface-mounted PMSM, L_d and L_q are almost equal. Therefore, T_E can be described as follows:

$$T_E = \frac{3}{2}p\psi_f i_q = K_t i_q \tag{4}$$

where K_t is the torque constant. On the other hand, the parasitic torque pulsation T_R is mainly caused by cogging torque, flux harmonics, and the current offset. According to the analysis presented in [27], the torque pulsation can be expressed simply as follows:

$$T_R = \sum_{n=1}^{\infty} k_n^s \sin(np\theta) + k_n^c \cos(np\theta) \tag{5}$$

where k_n^s and k_n^c are the n^{th} harmonic amplitudes. In practice, the high-order harmonics are usually ignored due to the inertia characteristic of load. Assume that the $1^{st}, 2^{nd}, \ldots N_h^{th}$ harmonics are the major harmonics that affect the torque ripple. These order harmonics can be obtained by analyzing the motor torque or current waveform as presented in the Appendix. A. The dynamic model (2) is rewritten as follows:

$$\dot{\omega} = -\frac{F}{J}\omega + \frac{K_t}{J} i_q + \frac{1}{J}\sum_{n=1}^{N_h} k_n^s \sin(n\theta_e) + k_n^c \cos(n\theta_e) - \frac{1}{J}T_L = a\omega + b i_q + d \tag{6}$$

where $a = -\dfrac{F}{J}$, $b = \dfrac{K_t}{J}$ and d represents the lumped disturbance which consists of the torque pulsation and the external load torque.

$$d = \frac{1}{J}\left(-T_L + \sum_{n=1}^{N_h} k_n^s \sin(n\theta_e) + k_n^c \cos(n\theta_e)\right) \tag{7}$$

It can be observed that d is a time-varying disturbance. Therefore, to facilitate the design of the observer, we express the lumped disturbance d as follows:

$$d = \frac{1}{J}\begin{bmatrix} 1 \\ \sin(\theta_e) \\ \cos(\theta_e) \\ \vdots \\ \sin(N_h\theta_e) \\ \cos(N_h\theta_e) \end{bmatrix}^T \begin{bmatrix} -T_L \\ k_1^s \\ k_1^c \\ \vdots \\ k_{N_h}^s \\ k_{N_h}^c \end{bmatrix} = f^T \rho \tag{8}$$

where

$$\begin{aligned} f &= \frac{1}{J}\big[1,\ \sin(\theta_e),\ \cos(\theta_e), \ldots,\ \sin(N_h\theta_e),\ \cos(N_h\theta_e)\big]^T \\ \rho &= \big[-T_L,\ k_1^s,\ k_1^c, \ldots,\ k_{N_h}^s,\ k_{N_h}^c\big]^T \end{aligned} \tag{9}$$

In this way, the time-varying disturbance d can be separated into two components: f, a vector measurable using position feedback, and ρ, a vector representing the external load torque and the amplitudes of the major harmonics. This characteristic will be utilized to determine the lumped disturbance d in the next section through the estimation of vector ρ.

III. DESIGN OF PERIODIC DISTURBANCE OBSERVER

According to the aforementioned analysis, the speed model of PMSM is consistently affected by periodic disturbances, which can be represented by the constant vector ρ. Hence, a PDOB is developed based on the Lyapunov stability theory to achieve a fast and accurate estimation of the unknown vector ρ. Compared to PIR [8], RC [25], and ILC [27], the proposed observer can handle a wide range of harmonic orders and is easy to implement. First, the speed model of PMSM can be rewritten as follows:

$$\dot{x}(t) = ax(t) + bu(t) + f^T(t)\rho \tag{10}$$

where $x(t) = \omega(t)$ and $u(t) = i_q(t)$. Then, the state-space model of PDOB is proposed as:

$$\dot{\hat{x}}(t) = ax(t) + b(u(t) - u_c(t)) + f^T\hat{\rho}(t) \tag{11}$$

where $\hat{x}(t)$ and $\hat{\rho}(t)$ represent the estimated values of $x(t)$ and ρ, respectively; and u_c denotes a compensation control signal. Define the observation errors as:

$$\begin{cases} e_x(t) = x(t) - \hat{x}(t) \\ e_\rho(t) = \rho - \hat{\rho}(t) \end{cases} \tag{12}$$

From (11) and (12), the derivative of the observation error is expressed as:

$$\begin{cases} \dot{e}_x(t) = bu_c(t) + f^T(t)e_\rho(t) \\ \dot{e}_\rho(t) = -\dot{\hat{\rho}}(t) \end{cases} \tag{13}$$

Proposition 1: Define the update law for $\hat{\rho}(t)$ as:

$$\hat{\rho}(t) = K_\rho f(t)x(t) - \xi(t) \tag{14}$$

where K_ρ is a positive constant and $\xi(t)$ is an auxiliary variable that is given by:

$$\dot{\xi}(t) = K_\rho f(t)\big(ax(t) + bu(t) + f^T(t)\hat{\rho}(t)\big) + K_\rho \dot{f}(t)x(t) - f(t)e_x(t) \tag{15}$$

Then, under update law (14), the observer will be stable.

Proof: According to (14), the derivative of e_ρ is rewritten as:

$$\begin{aligned} \dot{e}_\rho(t) &= -K_\rho f(t)\dot{x}(t) - K_\rho \dot{f}(t)x(t) + \dot{\xi}(t) \\ &= -K_\rho f(t)\big(ax(t) + bu(t) + f^T(t)\rho\big) \\ &\quad + K_\rho f(t)\big(ax(t) + bu(t) + f^T(t)\hat{\rho}(t)\big) - f(t)e_x(t) \\ &= -K_\rho f(t)f^T(t)e_\rho(t) - f(t)e_x(t) \end{aligned} \tag{16}$$

To illustrate the stability of PDOB, a Lyapunov candidate function (LCF) is proposed as follows:

$$V = \frac{1}{2}e_\rho^T(t)e_\rho(t) + \frac{1}{2}e_x^2(t) \tag{17}$$

Then, the derivative of LCF can be expressed as follows:

$$\begin{aligned} \dot{V} &= e_\rho^T(t)\dot{e_\rho}(t) + e_x(t)\dot{e_x}(t) \\ &= e_\rho^T(t)\big(-K_\rho f(t)f^T(t)e_\rho(t) - f(t)e_x(t)\big) \\ &\quad + e_x(t)\big(bu_c(t) + f^T(t)e_\rho(t)\big) \\ &= -K_\rho e_\rho^T(t)f(t)f^T(t)e_\rho(t) + e_x(t)bu_c(t) \end{aligned} \tag{18}$$

To satisfy the Lyapunov stability theory, $\dot{V}(k)$ must be negative. Therefore, the compensation signal $u_c(t)$ can be calculated as follows:

$$u_c(t) = -b^{-1}K_x e_x(t) \tag{19}$$

where $K_x > 0$. Then, the derivative (18) is rewritten as:

$$\dot{V} = -K_\rho e_\rho^T(t)f(t)f^T(t)e_\rho(t) - K_x e_x^2(t) \le 0 \tag{20}$$

Therefore, Proposition 1 is proved. □

In (19), the gain K_x will affect the convergence behavior of the observer. Ideally, it should be chosen as large as possible to ensure fast convergence. However, a high value of K_x can result in significant fluctuations in the compensation signal u_c. Assume that $\kappa_1 \le K_x \le \kappa_2$, where κ_1 and κ_2 are positive constants representing the desired margin for K_x. Then, the range of the compensation signal is expressed as:

$$\begin{cases} -b^{-1}(\kappa_2 + a)e_x(t) \le u_c(t) \le -b^{-1}(\kappa_1 + a)e_x(t) \\ \quad \text{if } e_x(t) \ge 0 \\ -b^{-1}(\kappa_1 + a)e_x(t) \le u_c(t) \le -b^{-1}(\kappa_2 + a)e_x(t) \\ \quad \text{if } e_x(t) < 0 \end{cases} \tag{21}$$

Define two auxiliary variables u_{c1} and u_{c2} as follows:

$$\begin{aligned} u_{c1}(t) &= \begin{cases} -b^{-1}(\kappa_2 + a)e_x(t) & \text{if} \quad e_x(t) \ge 0 \\ -b^{-1}(\kappa_1 + a)e_x(t) & \text{if} \quad e_x(t) < 0 \end{cases} \\ u_{c2}(t) &= \begin{cases} -b^{-1}(\kappa_2 + a)e_x(t) & \text{if} \quad e_x(t) \ge 0 \\ -b^{-1}(\kappa_1 + a)e_x(t) & \text{if} \quad e_x(t) < 0 \end{cases} \end{aligned} \tag{22}$$

Then the constraints (21) can be simply rewritten as follows:

$$u_{c1}(t) \le u_c(t) \le u_{c2}(t) \tag{23}$$

In the following section, the values of K_x and u_c are optimized to obtain the best performance.

IV. DESIGN OF THE EMPSC

After estimating the periodic disturbance by using PDOB, the design of the EMPSC is presented in this section. The control diagram of EMPSC is illustrated in Fig. 1. The main objective of EMPSC is to determine the optimal current reference to achieve the best speed-tracking performance. At each sampling instant, the optimal current is calculated by minimizing a cost function (CF). First, a mathematical discrete-time model is employed to predict the future behavior of the system. Then, a quadratic cost function is formulated to evaluate the control performance. Finally, an explicit process is presented for minimizing the cost function while reducing computational complexity.

A. DISCRETE-TIME PREDICTION MODEL

The speed model and observer model are expressed in discrete-time domain as follows:

$$x(k+1) = Ax(k) + Bu(k) + F(k)\rho \tag{24}$$

$$\hat{x}(k+1) = Ax(k) + B\bar{u}(k) + F(k)\hat{\rho} \tag{25}$$

where $A = (1 + aT_s)$, $B = bT_s$, $F(k) = f(k)T_s$, $\bar{u}(k) = u(k) + u_c(k)$ and T_s is the sample time. Let N_P denote the prediction horizon. Due to the convergence of PDOB, the observer model (23) is employed to establish the prediction model and predict the future states as follows:

$$\begin{aligned} x(k+1|k) &= Ax(k) + B\bar{u}(k) + F^T(k)\hat{\rho}(k) \\ x(k+2|k) &= Ax(k+1|k) + B\bar{u}(k+1) + F^T(k+1)\hat{\rho}(k) \\ &\vdots \\ x(k+N_p|k) &= Ax(k+N_p-1|k) + B\bar{u}(k+N_P-1) \\ &\quad + F^T(k+N_p-1)\hat{\rho}(k) \end{aligned} \tag{26}$$

where $\bar{u}(k+i|k)$ and $x(k+i|k)$ denote ith step ahead predicted states from time instant k of $\bar{u}(k)$ and $x(k)$ respectively. Furthermore, vector $F(k)$ is slow dynamic and can be considered as a constant vector during the prediction horizon. Let $\epsilon(k) = F^T(k)\hat{\rho}$, the prediction model (26) is rewritten in matrix form as:

$$X(k) = Hx(k) + \Phi_u U(k) + \Phi_\epsilon \epsilon(k) \tag{27}$$

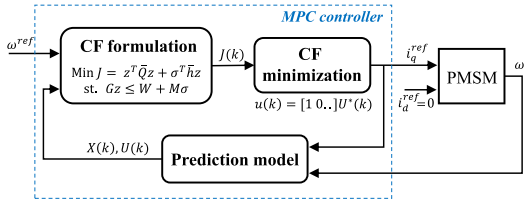

FIGURE 1. Control diagram of MPC for PMSM.

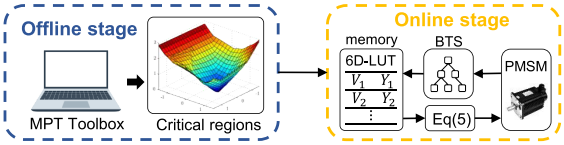

FIGURE 2. Explicit MPC methodology.

where prediction vectors $X(k)$, $U(k)$ and matrices H, Φ_u, and Φ_ϵ are given by:

$$X(k) = \left[x(k+1|k), x(k+2|k), \ldots, x(k+N_p|k)\right]^T$$
$$U(k) = \left[\bar{u}(k|k), \bar{u}(k+1|k), \ldots, \bar{u}(k+N_p-1|k)\right]^T$$
$$H = \begin{bmatrix} A \\ A^2 \\ \vdots \\ A^{N_p} \end{bmatrix} \quad \Phi_u = \begin{bmatrix} B & 0 & \cdots & 0 \\ AB & B & \cdots & 0 \\ \vdots & & & \vdots \\ A^{N_p-1}B & A^{N_p-2}B & \cdots & B \end{bmatrix}$$
$$\Phi_\epsilon = \begin{bmatrix} 1 \\ A \\ \vdots \\ A^{N_p-1} + A^{N_p-2} + \cdots + 1 \end{bmatrix} \tag{28}$$

B. MODIFIED COST FUNCTION FORMULATION

In conventional MPC, to evaluate the control performance, the cost function is usually established by a quadratic form as follows:

$$J_c(k) = \big(X_d(k) - X(k)\big)^T Q\big(X_d(k) - X(k)\big) + U^T(k)RU(k) \tag{29}$$

where Q, and R are symmetric positive definite (denoted > 0) weighting matrices, $X_d(k)$ is reference vector. By optimizing $J_c(k)$, the optimal control signal $U^*(k)$ will result in the prediction model with good tracking performance. However, the prediction model is established based on the estimated value of ρ as described in (24) and (25). Consequently, estimation errors can degrade the performance of the actual speed model compared to the prediction model. This performance difference is significant when the observer has not reached a stable state, such as in a speed transition state or when the external load torque suddenly occurs. To maintain the performance of the real system, a modified cost function with an additional terminal term is proposed as follows:

$$J(k) = J_c(k) + \big(x(k+1) - x(k+1|k)\big)^2 \tag{30}$$

where the additional term $\big(x(k+1) - x(k+1|k)\big)^2$ expresses the difference between the prediction model $x(k+1|k)$ and the actual model $x(k+1)$. Thus, the addition of this term into the cost function will ensure the performance of the actual model, and reduce the influence of the estimation error. Considering the speed model and the PDOB model, the predicted state $x(k+1|k)$ is described as follows:

$$\begin{aligned} x(k+1|k) &= Ax(k) + B(u(k) + u_c(k)) + F^T(k)\hat{\rho}(k) \\ &= x(k+1) + Bu_c(k) + F^T(k)(\hat{\rho}(k) - \rho) \end{aligned} \tag{31}$$

Besides, the speed model (24) at time instant $k-1$ given by:

$$x(k) = Ax(k-1) + Bu(k-1) + F^T(k-1)\rho \tag{32}$$

and combine with assumption that $F(k)$ is a slow dynamic vector $\big(F(k) \approx F(k-1)\big)$, the equation (31) is rewritten as:

$$x(k+1|k) = x(k+1) + Bu_c(k) + d_x \tag{33}$$

where d_x is a certain part given by:

$$d_x = F^T(k)\hat{\rho}(k) - x(k) + Ax(k-1) + Bu(k-1) \tag{34}$$

Then, the CF (30) is reformulated as:

$$\begin{aligned} J(k) = B^2u_c^2(k) + 2Bd_xu_c(k) + U^T(k)\big(\Phi_u^TQ\Phi_u + R\big)U(k) \\ + 2\Phi_u^TQ\big(Hx(k) + \Phi_\epsilon\epsilon(k) - X_d\big)U(k) + C \end{aligned} \tag{35}$$

where $u_c(k)$ and $U(k)$ are the optimal variables; C is a component independent of the optimal variables and can be ignored in the cost function. Furthermore, one of the advantage of MPC is dealing with constraints. In design of EMPSC, the constraints of $J(k)$ are set as:

$$i_q^{min} \le u(k+i) \le i_q^{max} \tag{36}$$

where i_q^{min} and i_q^{max} represent the constraints on the control signal $u(k)$. By using the constraint (36), the motor will be ensured that operate in normal stages and avoid overloading. Combined with the condition (23) for the compensation signal, the optimal control signal is computed as the solution of the following QP optimization problem:

$$\begin{aligned} \min_{u_c(k),U(k)} \quad & J(k) = B^2u_c^2(k) + U^T(k)\big(\Phi_u^TQ\Phi_u + R\big)U(k) \\ & + 2Bd_xu_c(k) + 2\Phi_u^TQ\big(Hx(k) + \Phi_\epsilon\epsilon(k) - X_d\big)U(k) \\ \text{subject to: } & i_q^{min} \le u(k+i) \le i_q^{max} \quad i = 0, 1, ..(N_p-1) \\ & u_{c1} \le u_c(k) \le u_{c2} \end{aligned} \tag{37}$$

In the MPC framework, according to the receding horizon principle, only the first component in the optimal sequence control vector $U(k)$ is applied to the optimal control signal. The current reference is then calculated as follows:

$$i_q^{ref}(k) = u^*(k) = [1,\ 0, \ldots\ 0]U^*(k) - u_c^*(k) \tag{38}$$

where $U^*(k)$ and $u_c^*(k)$ are the optimal solutions of QP problem (37).

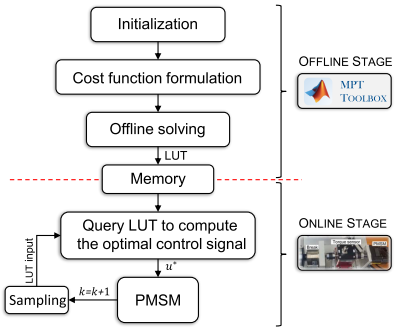

FIGURE 3. Flowchart for EMPSC.

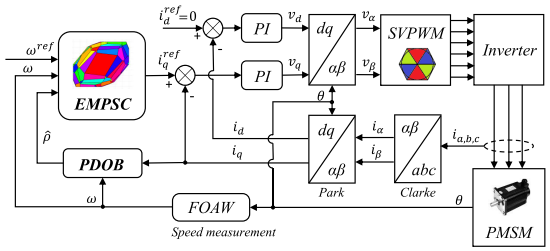

FIGURE 4. Structure block diagram of the proposed EMPSC.

TABLE 1. The proposed control algorithm.

Online iteration algorithm of overall control structure
1. Set $k = 1$.
2. Measure the speed and current feedback.
3. Update the estimated vector $\hat{\rho}(k)$ according to (14)
4. Calculate vector $\sigma(k)$ and consult explicit LUT to determine the optimal solution.
5. Implement FOC with the current reference $i_q^{ref} = u^*(k)$ and $i_d^{ref} = 0$.
6. Set $k = k + 1$, and go to step. 2.

C. EXPLICIT PROCESS

As aforementioned, the optimal control signal is calculated by solving the QP optimization problem (37) at each sampling instant. However, solving online QP problems usually requires a significant computational effort and can be challenging to implement in real-time. In this section, an explicit process is introduced to efficiently solve online optimization problems. First, the optimization problem is reformulated as follows:

$$\begin{aligned} \text{OP:} \quad & \min_{z(k)} J(k) = \frac{1}{2} z^T(k) \bar{Q} z(k) + \sigma^T(k) \bar{h}^T z(k) \\ & \text{subject to: } Gz(k) \leq W + M\sigma(k) \end{aligned} \tag{39}$$

where weighting matrices $\bar{Q}$, $\bar{h}$, G, W and M are given in the Appendix. B; vector $z(k)$ denotes the optimal variables and $\sigma(k)$ is a parametric vector representing parameters in the optimization problem.

$$\begin{aligned} z(k) &= [u_c(k) \quad U(k)]^T \in R^{N_p+1} \\ \sigma(k) &= [d_x(k),\ x_d(k),\ x(k),\ \epsilon(k),\ u_{c1}(k),\ u_{c2}(k)]^T \in R^6 \end{aligned} \tag{40}$$

The key idea of explicit MPC is to pre-solve the QP offline for the entire set of the parametric vector $\sigma(k)$ to obtain the universal optimizer function $z(k)$, which only depends on $\sigma(k)$. The explicit MPC consists of two stages:

1) Offline stage: In this stage, the optimization problem (39) is pre-computed using the multi-parametric programming (MPP) algorithm [30] over the feasible set of parametric $\sigma(k)$. The optimal solution is defined as a continuous and piecewise affine (PWA) state-feedback law:

$$z^*(k) = \begin{cases} V_1\sigma(k) + Y_1 & \text{if } \sigma(k) \in \mathcal{P}_1 \\ \vdots & \\ V_{\mathcal{I}}\sigma(k) + Y_{\mathcal{I}} & \text{if } \sigma(k) \in \mathcal{P}_{\mathcal{I}} \end{cases} \tag{41}$$

where $\mathcal{P}_i (i = 1, \ldots, \mathcal{I})$ represents $\mathcal{I}$ nonoverlapped active regions; the matrices V_i and Y_i are obtained through the MPP algorithm. The condition for the parametric vector $\sigma(k)$ to fall into the ith region is:

$$\sigma(k) \in \mathcal{P}_i \quad \text{if} \quad \mathcal{H}_i\sigma(k) \leq \mathcal{K}_i \tag{42}$$

with $\mathcal{H}_i$ and $\mathcal{K}_i$ are also given by the MPP algorithm. The pairs $(V_i, Y_i, \mathcal{H}_i, \mathcal{K}_i)$ are used to formulate the optimal solution law and stored in a look-up table (LUT).

2) Online stage: The task of the online stage involves searching for the active region that contains the current parametric vector by evaluating the condition (42). Then, the LUT is retrieved to compute the optimal solution using equation (38).

The explicit process is illustrated in Fig. 2. In our implementation, the multi-parametric toolbox (MPT) [35] is employed in Matlab environment to offline solve the MPP problem (39) and export the PWA solution to the LUT. Additionally, the binary tree search (BTS) method [36] is also utilized to reduce the search time in the online stage. The flowchart of EMPSC is shown in Fig. 3.

D. OVERALL CONTROL STRUCTURE

Fig. 4 illustrates the overall control structure diagram of the proposed EMPSC for PMSM. This structure is built from the cascaded field-oriented control (FOC), where the proposed EMPSC is employed as the speed controller for calculating the reference for the q-axis current, while the PI controller is used for the current loop. The speed controller consists of two main blocks:

1) The PDOB for fast and accurate estimation of the lumped periodic disturbance in the dynamic model.
2) The EMPSC for computing the optimal current reference i_q^{ref}, which can achieve good control performance and reduce the torque ripple.

The real-time implementation of the proposed control strategy is summarized in the following Table 1.

V. IMPLEMENTATION AND SIMULATION STUDY

To evaluate the control performance of the proposed methodology, a simulation model has been constructed using

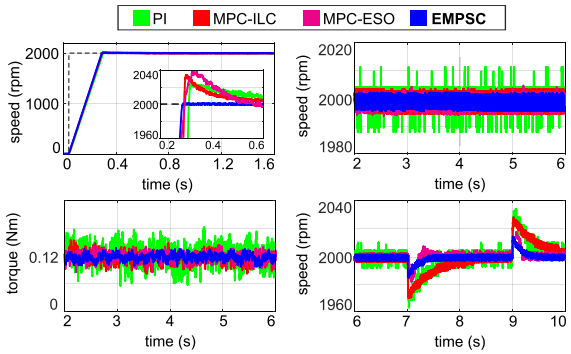

FIGURE 5. Simulation results of the three methods under a step speed profile and the load torque suddenly occurs.

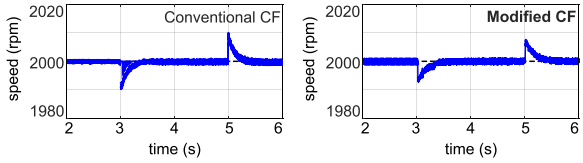

FIGURE 6. Effective of the modified cost function.

TABLE 2. PMSM parameters.

Parameter	Value	Parameter	Value
Rated power	30 W	Limited current	6.5 A
Rated voltage	24 V	Pole pairs	5
Rated speed	3000 rpm	K_t	0.0613 Nm/A
R_s	1.4 Ω	J	3.386×10^{-4} kg·m^2
L_q, L_q	1.12 mH	B	6×10^{-4} Nm·s/rad

Matlab/Simulink. The details of the PMSM model, including the presence of torque ripple, are is built based on the FEA model [36]. The motor parameters are listed in Table 2.

A. TUNING GUIDELINES FOR CONTROLLER GAINS

The control gains are presented in Table 3. An important parameter of EMPSC is the prediction horizon length N_p. In theory, the length N_p should be selected to be as long as possible to optimize performance. However, in practical applications, a very long N_p will significantly increase the computational complexity of MPC-based algorithms. In this paper, $N_p = 8$ is chosen based on an evaluation of the computational capabilities of the hardware system. Weighting matrices Q and R in the cost function are selected by trading off between control performance and control effort. A large value of Q provides a fast-tracking ability, while a large value of R implies an energy-efficient controller. Yamashita's guideline [37] suggests a simple selection of $Q = I$ and $R = \alpha I$, where α is a very small value. Here, we use $\alpha = 0.01$. The major harmonics in PDOB design are presented in Appendix. A. The parameters of the PDOB (K_ρ, κ_1, and κ_2) are tuned by evaluating the simulation and experimental results. Across results conducted in the entire admissible speed range, it is observed that $K_\rho \in [15; 50]$, $\kappa_1 \in [2; 10]$, and $\kappa_2 \in [20; 45]$ achieve better performance.

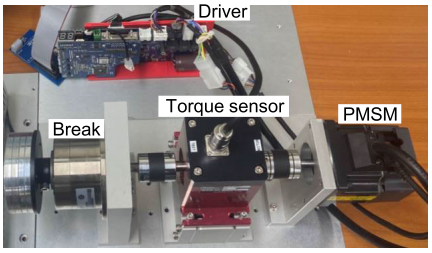

FIGURE 7. Experimental PMSM platform.

TABLE 3. Parameters of the proposed EMPSC.

parameter	value	parameter	value	parameter	value
K_ρ	25	κ_1	5	κ_2	30
Q	I_8	R	$0.01I_8$	N_p	8

B. IMPLEMENTATION AND SIMULATION RESULTS

To assess the control performance of the proposed methodology, three additional control strategies were employed for comparison: a conventional PI speed controller, an MPC based on iterative learning control (MPC-ILC) [27], and an MPC based on extended state observer (MPC-ESO) [28]. The parameters of the PI controller were tuned using the pole-zero cancellation technique with a cut-off frequency of 125 Hz. Additionally, an anti-windup compensation strategy [38] was applied in the PI controller to mitigate the effect of the integrated component during speed jumping. For a fair comparison, the MPC-ILC and MPC-ESO control methods were also implemented in the simulation environment. The MPC-ILC and MPC-ESO methods are recently published MPC papers for torque ripple minimization, and they also have a similar structure to the proposed EMPSC. All the control schemes adopted the FOC architecture and utilized the same PI current controller, which was tuned using the pole-zero cancellation technique at 1000 Hz. In the simulation setup, the sampling times for the current and speed controllers were set at 50 μs and 0.5 ms, respectively. Furthermore, the influence of quantization speed errors caused by the encoder was taken into consideration. To model this effect, a 20000 pulse/rev encoder block was integrated into the position feedback signal.

In the following simulation study, the PMSM is assumed to operate at a speed of 2000 rpm with an external load torque of 0.1 Nm applied from 7 s to 9 s. The simulation results obtained from the three methods are depicted in Fig. 5. As shown in Fig. 5, the proposed EMPSC exhibits better performance with zero overshoot, the shortest settling time, minimized speed-torque ripple, and reduced speed fluctuation induced by the external load torque.

C. MODIFIED COST FUNCTION

As mentioned in Section IV, the modified cost function is proposed to reduce the influence of estimation error. To validate the effectiveness of the modified cost function, the motor system is tested at 2000 rpm and the load torque of 0.1 Nm is applied. In this test, the estimation errors at

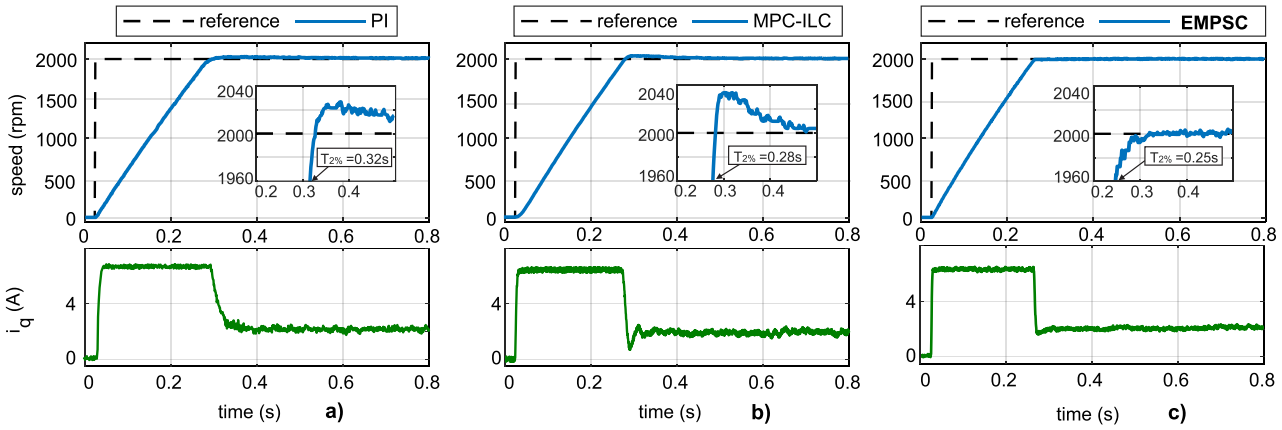

FIGURE 8. Comparative experimental results. Dynamic performance. a) PI controller, b) MPC-ILC, c) EMPSC.

TABLE 4. Computation efficiency comparison.

Algorithm	Matlab toolbox	CasADi	RNN	EMPC
Computation time	9.8 ms	3.2 ms	0.18 ms	0.02 ms

times that load torque applied and released are significant. Thus, by evaluating the motor behavior, we can verify the impact of the modified cost function. Fig. 6 shows the speed performance comparison between the modified cost function and the conventional cost function. As can be observed in Fig. 6, the modified cost function exhibits better performance, reducing speed fluctuation compared to the conventional cost function. Therefore, the modified cost function enhances the robustness of the proposed control strategy against external disturbances.

D. COMPUTATION EFFICIENCY COMPARISON

To assess the feasibility of implementing the proposed method in a real system, we evaluate the computation time of EMPSC in this section. Table 4 presents a comparison of the computation time for EMPSC with other algorithms commonly used for deploying MPC, such as the Matlab toolbox (active-set), the CasADi package (interior-point) [39], and RNN [19]. All simulations were conducted on a PC equipped with an AMD 3500x CPU, 32GB RAM, and an RTX 3050 GPU. The comparison in Table 4 reveals that the Matlab toolbox and CasADi require a significant amount of time to solve the optimization problem, limiting their practical applicability, especially in high-frequency sampling systems. The RNN algorithm has been successfully applied in real implementation but is most suitable for short-horizon controllers (e.g., $N_p = 5$ in [19]), and it also exhibits longer execution times when applied to long-horizon MPC. In contrast, EMPC exhibits an average execution time of only 0.02 ms, making it highly suitable for real-time implementation.

VI. EXPERIMENT RESULTS

This section provides a comprehensive description of the laboratory experimental setup of a VSI-fed PMSM drive prototype to investigate the effectiveness of the proposed EMPSC. Subsequently, the experimental results compared with the conventional PI and MPC-ILC are presented.

A. EXPERIMENTAL TEST BENCH SETUP

Fig. 7 depicts the experimental hardware setup of the PMSM platform. The test motor is a 30W servo brushless with the parameters listed in Table 2. The rotor position is measured via an incremental optical encoder with a resolution ratio of 20000 pulses/rev. The speed feedback is accurately calculated by using the first-order adaptive window (FOAW) method [40]. A coaxially mounted RCS-20KC torque sensor is utilized to measure the generated torque. The load side comprises load disks for inertia adjustment and a ZKG-20AN Mitsubishi powder clutch to generate external load torque TL. The CTA3200 board is used to control the powder clutch. The control algorithm is implemented using a C-program in the arm cortex STM32F446VC-based motor drive. The sampling times of the speed controller and current controller are 0.5 ms and 50 μs, respectively. The switching frequency for the SV-PWM inverter is set to 50 kHz. All experimental data are transmitted from the motor driver to a computer using RS232 communication.

B. CONTROL PERFORMANCE COMPARISON

1) DYNAMIC PERFORMANCE

First, the speed-tracking performance of the three control schemes is verified. A step speed reference of 2000 rpm is commanded. In this test, the dynamic performance is revealed through the overshoot and settling time of the speed response. The experimental results obtained from the three methods are shown in Fig. 8. It can be seen that the PI speed controller exhibits poor dynamic performance with a speed overshoot of 28 rpm and a settling time of 0.32 s. Despite the addition of the anti-windup compensator, the PI controller still inevitably generates a larger overshoot due to the impact of the integral part. The speed feedback of MPC-ILC shows a faster dynamic response of 0.28 s but the speed overshoot is still significant. The reason for this weakness is that the MPC-ILC ignores the current

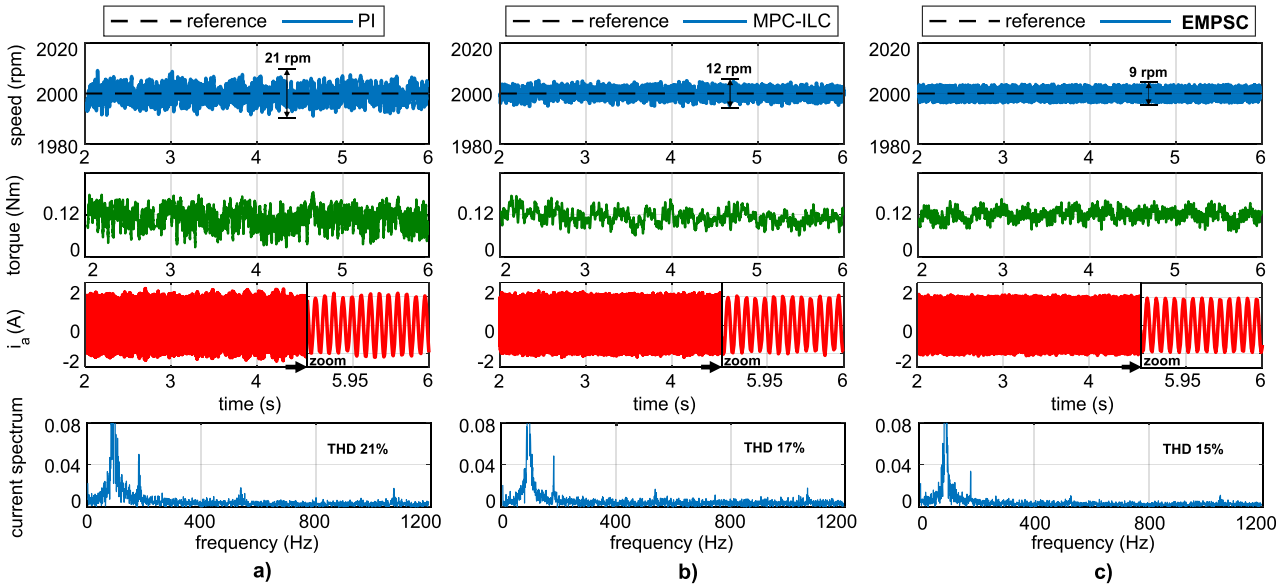

FIGURE 9. Comparative experimental results. Steady-state performance. a) PI controller, b) MPC-ILC, c) EMPSC.

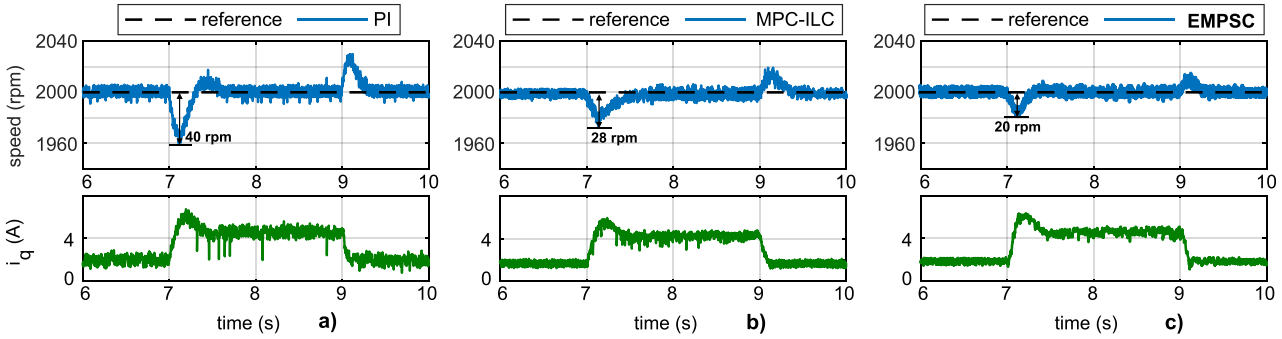

FIGURE 10. Comparative experimental results. Anti-fluctuation performance. a) PI controller, b) MPC-ILC, c) EMPSC.

limitations in control design. Consequently, when the current becomes saturated during the speed-raising phase, the control performance of MPC-ILC is diminished. On the other hand, as depicted in Fig. 8c, the proposed EMPSC can achieve good dynamic performance with zero overshoot and the fastest settling time. By considering current constraints in the control design, the proposed EMPSC has overcome the overshoot problem in MPC-ILC. Additionally, the short settling time of EMPSC and MPC-ILC in this test also demonstrates the fast dynamic response ability of the MPC-based control method.

2) STEADY-STATE PERFORMANCE

To evaluate the torque ripple minimization performance of the three methods during the steady-state, the reference speed of 2000 rpm is maintained from 2s to 6s. In this test, the generated torque and the stator current are also analyzed. To quantitatively measure the torque ripple, the torque ripple factor (TRF) is defined in [12] as follows:

$$TRF(\%) = \frac{T_{pk-pk}}{T_{rated}} \times 100 \tag{43}$$

where T_{pk-pk} represents the peak-to-peak torque ripple, and T_{rated} is the rated value of the electromagnetic torque. Additionally, the peak-to-peak value of speed ripple (SR) and the total harmonic distortion (THD) of the stator current are also employed to compare the control performance of the three methods. The experimental results are shown in Fig. 9. As shown in Fig. 9a, the conventional PI controller reveals poor steady-state performance, resulting in large speed oscillation (SR 21 rpm), large torque ripple (TRF 37.5%), and significant current harmonics (THD 21%). In contrast, the experimental results obtained from MPC-ILC and the EMPSC demonstrate excellent torque ripple minimization performance. Especially, the proposed EMPSC achieves a slightly better control performance on in terms of both speed oscillation, torque ripple, and current distortion.

Moreover, to ensure the torque ripple minimization performance across different speed ranges, the three methods are also evaluated at speeds of 300 rpm, 1200 rpm, 2000 rpm, and 3000 rpm. The experimental results are summarized in Table 5, where the values of speed ripple, torque ripple factor, and current THD are observed to evaluate the three methods. As shown in Table 5, the proposed EMPSC exhibits superior

TABLE 5. Steady-state performance comparison of the three methods.

Index	Speed (rpm)	PI	MPC-ILC	EMPSC
SR (rpm)	300	16	11	10
	1200	18	13	11
	2000	21	12	9
	3000	22	15	12
TRF (%)	300	32.1	24.6	21.8
	1200	36.2	25.8	21.5
	2000	37.5	24.5	22.9
	3000	40.7	26.6	23.5
THD (%)	300	21.6	15.4	13.8
	1200	23.2	16.5	14.5
	2000	21.1	16.9	15.2
	3000	22.5	17.8	16.1

performance in torque ripple minimization, speed smoothing, and current harmonic rejection across the entire speed range.

3) ANTI-FLUCTUATION PERFORMANCE

Finally, to demonstrate the robustness of the proposed EMPSC, an experiment is conducted using a powder clutch to generate an external load torque of $T_L = 0.1$ Nm from 7 s to 9 s. Fig. 10 compares the anti-fluctuation performance of the three methods. As depicted in Fig. 10a, the conventional PI controller reveals a significant speed error when the load torque is applied and released, with a speed fluctuation of 40 rpm. The experimental results obtained from MPC-ILC also exhibit a large speed fluctuation of 28 rpm. These experimental results demonstrate the weak robustness of both the PI controller and MPC-ILC against external disturbances. On the other hand, by considering the disturbance in the observer design, the proposed method provides strong robustness with the smallest speed error of 20 rpm.

Through the above-mentioned experiments, the effectiveness of the proposed method has been verified. When compared to the PI controller and MPC-ILC, the proposed method achieves better speed-tracking performance, stronger robustness against disturbances, and notably, a superior torque ripple minimization capacity.

VII. CONCLUSION

This paper proposes a simple EMPSC control structure to improve the performance of PMSM with torque ripple minimization. The main contributions of this study are as follows: 1) The design of PDOB has been proposed for the online estimation of parasitic torque pulsation in PMSM. 2) An EMPSC with a novel cost function is proposed to enhance the control performance and suppress the torque ripple. The computational volume of the entire control scheme has also been taken into account to ensure the real-time implementation of the proposed method. The simulation and experimental results demonstrate the practicability of the proposed control method with performance improvements such as the removal of speed overshoot, a substantial 39% reduction in torque ripple, and a remarkable 28% decrease in current distortion compared to the conventional FOC method. Moreover, the robustness against external disturbances was also verified with a reduction in speed fluctuation by 50%.

Future work based on this paper may consist of:

1) Improve EMPSC with considering the parameters mismatches.
2) Extend EMPSC for current control.

APPENDIX A
ANALYSIS OF TORQUE RIPPLES

Torque ripple in PMSMs primarily arises from three sources: cogging torque, flux harmonics, and current measurement errors. According to research [10], [27], a brief analysis of these sources is presented below:

1) Cogging torque: Cogging torque emerges due to the interaction between the magnetic flux and stator slots. It can be represented by a Fourier series as follows:

$$T_{cog} = \sum_{k=1}^{\infty} T_{cog}^{k} \sin(mk\theta_e) \tag{44}$$

where T_{cog}^{k} is the Fourier coefficients, m represents the least common multiple of stator slots N_s and the number of poles $2p$. In the case of our PMSM, $N_s = 6$ and $p = 5$, yielding $m = 30$. Consequently, the orders of cogging torque include 6, 12, 18,..

2) Flux harmonics: Flux harmonics result from the nonsinusoidal distribution of flux density in the air gap. The torque ripple associated with flux harmonics is expressed as follows:

$$T_{flux} = \sum_{k=1}^{\infty} T_{flux}^{k} \cos(6k\theta_e) \tag{45}$$

where T_{cog}^{k} is the $(6k)^{th}$ harmonic amplitude.

3) Current measurement error: The DC offset in stator current measurements and scaling errors also contribute to pulsating torque at specific frequencies.

$$T_{cur} = k_{ce}\left(\cos(2\theta_e + \frac{\pi}{3}) + \frac{1}{2}\right) \tag{46}$$

where k_{ce} is the current measurement error factor.

Combining (45), (46), and (47), it can be concluded that torque ripple consists of harmonic components such as the 2nd, 6th, 12th,...

Furthermore, based on the FFT analysis of the stator current, as shown in Fig. 9, the major harmonic components of torque ripple in our PMSM test bench are the 2nd, 6th, and 12th harmonics. Higher harmonics (above 12th) are disregarded due to the inertia characteristics of the load. Therefore, in our implementation, we focus on mitigating the major harmonics, specifically the 2nd, 6th, and 12th harmonics.

APPENDIX B
DEFINITION OF MATRICES

$$\bar{Q} = \begin{bmatrix} 2B^2 & [0]_{1\times N_p} \\ [0]_{N_p\times 1} & 2\Phi_u^T Q \Phi_u + R \end{bmatrix}$$

$$\bar{h} = \begin{bmatrix} B & 0 & 0 & 0 & 0 & 0 \\ 0 & -\Phi_u^T Q[1]_{N_p\times 1} & \Phi_u^T QH & \Phi_u^T Q\Phi_\epsilon & 0 & 0 \end{bmatrix}$$
$$G = \begin{bmatrix} G_1 \\ G_2 \end{bmatrix} \quad W = \begin{bmatrix} W_1 \\ W_2 \end{bmatrix} \quad M = \begin{bmatrix} M_1 \\ M_2 \end{bmatrix}$$
$$G_1 = \begin{bmatrix} -[1]_{N_p\times 1} & I_{N_p} \\ [1]_{N_p\times 1} & -I_{N_p} \end{bmatrix} \quad W_1 = \begin{bmatrix} [1]_{N_p\times 1} i^{max} \\ -[1]_{N_p\times 1} i^{min} \end{bmatrix}$$
$$M_1 = \begin{bmatrix} 0 \end{bmatrix}_{2N_p\times 6}$$
$$G_2 = \begin{bmatrix} 1 & [0]_{1\times N_p} \\ -1 & [0]_{1\times N_p} \end{bmatrix} \quad W_2 = \begin{bmatrix} 0 \\ 0 \end{bmatrix}$$
$$M_2 = \begin{bmatrix} 0 & 0 & 0 & 0 & 0 & 1 \\ 0 & 0 & 0 & 0 & -1 & 0 \end{bmatrix} \tag{47}$$

where $G_1 z(k) \leq W_1 + M_1\sigma(k)$ represents $2N_p$ constraints in (36), which are used for limiting the value of control signal and $G_2 z(k) \leq W_2 + M_2\sigma(k)$ is the condition (21) for the compensation signal u_c.

REFERENCES

[1] K.-C. Kim, "A novel method for minimization of cogging torque and torque ripple for interior permanent magnet synchronous motor," *IEEE Trans. Magn.*, vol. 50, no. 2, pp. 793–796, Feb. 2014.

[2] W. Fei and P. C. Luk, "Torque ripple reduction of a direct-drive permanent-magnet synchronous machine by material-efficient axial pole pairing," *IEEE Trans. Ind. Electron.*, vol. 59, no. 6, pp. 2601–2611, Jun. 2012.

[3] M. Dai, A. Keyhani, and T. Sebastian, "Torque ripple analysis of a PM brushless DC motor using finite element method," *IEEE Trans. Energy Convers.*, vol. 19, no. 1, pp. 40–45, Mar. 2004.

[4] D. Wang, X. Wang, and S.-Y. Jung, "Cogging torque minimization and torque ripple suppression in surface-mounted permanent magnet synchronous machines using different magnet widths," *IEEE Trans. Magn.*, vol. 49, no. 5, pp. 2295–2298, May 2013.

[5] P. L. Chapman, S. D. Sudhoff, and C. A. Whitcomb, "Optimal current control strategies for surface-mounted permanent-magnet synchronous machine drives," *IEEE Trans. Energy Convers.*, vol. 14, no. 4, pp. 1043–1050, Dec. 1999.

[6] C. Lai, G. Feng, K. L. V. Iyer, K. Mukherjee, and N. C. Kar, "Genetic algorithm-based current optimization for torque ripple reduction of interior PMSMs," *IEEE Trans. Ind. Appl.*, vol. 53, no. 5, pp. 4493–4503, Sep. 2017.

[7] D. Flieller, N. K. Nguyen, P. Wira, G. Sturtzer, D. O. Abdeslam, and J. Merckl´e, "A self-learning solution for torque ripple reduction for nonsinusoidal permanent-magnet motor drives based on artificial neural networks," *IEEE Trans. Ind. Electron.*, vol. 61, no. 2, pp. 655–666, Feb. 2014.

[8] C. Xia, B. Ji, and Y. Yan, "Smooth speed control for low-speed high-torque permanent-magnet synchronous motor using proportional–integral–resonant controller," *IEEE Trans. Ind. Electron.*, vol. 62, no. 4, pp. 2123–2134, Apr. 2015.

[9] Z. Zhou, C. Xia, Y. Yan, Z. Wang, and T. Shi, "Disturbances attenuation of permanent magnet synchronous motor drives using cascaded predictive–integral–resonant controllers," *IEEE Trans. Power Electron.*, vol. 33, no. 2, pp. 1514–1527, Feb. 2018.

[10] G. Feng, C. Lai, and N. C. Kar, "A closed-loop fuzzy-logic-based current controller for PMSM torque ripple minimization using the magnitude of speed harmonic as the feedback control signal," *IEEE Trans. Ind. Electron.*, vol. 64, no. 4, pp. 2642–2653, Apr. 2017.

[11] J. Liu, H. Li, and Y. Deng, "Torque ripple minimization of PMSM based on robust ILC via adaptive sliding mode control," *IEEE Trans. Power Electron.*, vol. 33, no. 4, pp. 3655–3671, Apr. 2018.

[12] W. Qian, S. K. Panda, and J.-X. Xu, "Torque ripple minimization in PM synchronous motors using iterative learning control," *IEEE Trans. Power Electron.*, vol. 19, no. 2, pp. 272–279, Mar. 2004.

[13] B. Talbi, F. Krim, A. Laib, A. Sahli, and B. Babes, "A sugeno-fuzzy tuning approach of weighting factor in model predictive control for PV grid-tied PUC7 multi-level inverter," in *Proc. 3rd Int. Conf. Smart Grid Renew. Energy (SGRE)*, Mar. 2022, pp. 1–6.

[14] B. Babes, N. Hamouda, S. Kahla, H. Amar, and S. S. M. Ghoneim, "Fuzzy model based multivariable predictive control design for rapid and efficient speed-sensorless maximum power extraction of renewable wind generators," *Electr. Eng. Electromech.*, no. 3, pp. 51–62, May 2022.

[15] A. Bouafassa, L. Rahmani, B. Babes, and R. Bayindir, "Experimental design of a finite state model predictive control for improving power factor of boost rectifier," in *Proc. IEEE 15th Int. Conf. Environ. Electr. Eng. (EEEIC)*, Rome, Italy, Jun. 2015, pp. 1556–1561.

[16] N. Hamouda, B. Babes, S. Kahla, and Y. Soufi, "Real time implementation of grid connected wind energy systems: Predictive current controller," in *Proc. 1st Int. Conf. Sustain. Renew. Energy Syst. Appl. (ICSRESA)*, Tebessa, Algeria, Dec. 2019, pp. 1–6.

[17] N. Hamouda, B. Babes, S. Kahla, Y. Soufi, J. Petzoldt, and T. Ellinger, "Predictive control of a grid connected PV system incorporating active power filter functionalities," in *Proc. 1st Int. Conf. Sustain. Renew. Energy Syst. Appl. (ICSRESA)*, Tebessa, Algeria, Dec. 2019, pp. 1–6.

[18] O. Aissa, S. Moulahoum, I. Colak, B. Babes, and N. Kabache, "Analysis and experimental evaluation of shunt active power filter for power quality improvement based on predictive direct power control," *Environ. Sci. Pollut. Res.*, vol. 25, no. 25, pp. 24548–24560, Sep. 2018.

[19] T. T. Nguyen, H. N. Tran, T. H. Nguyen, and J. W. Jeon, "Recurrent neural network-based robust adaptive model predictive speed control for PMSM with parameter mismatch," *IEEE Trans. Ind. Electron.*, vol. 70, no. 6, pp. 6219–6228, Jun. 2023.

[20] Z. Ma, S. Saeidi, and R. Kennel, "FPGA implementation of model predictive control with constant switching frequency for PMSM drives," *IEEE Trans. Ind. Informat.*, vol. 10, no. 4, pp. 2055–2063, Nov. 2014.

[21] Z. Zhou, C. Xia, T. Shi, and Q. Geng, "Model predictive direct duty-cycle control for PMSM drive systems with variable control set," *IEEE Trans. Ind. Electron.*, vol. 68, no. 4, pp. 2976–2987, Apr. 2021.

[22] M. Wu, X. Sun, J. Zhu, G. Lei, and Y. Guo, "Improved model predictive torque control for PMSM drives based on duty cycle optimization," *IEEE Trans. Magn.*, vol. 57, no. 2, pp. 1–5, Feb. 2021.

[23] Y. Zhang and H. Yang, "Model predictive torque control of induction motor drives with optimal duty cycle control," *IEEE Trans. Power Electron.*, vol. 29, no. 12, pp. 6593–6603, Dec. 2014.

[24] S. Chai, L. Wang, and E. Rogers, "A cascade MPC control structure for a PMSM with speed ripple minimization," *IEEE Trans. Ind. Electron.*, vol. 60, no. 8, pp. 2978–2987, Aug. 2013.

[25] Y. Liu, S. Cheng, B. Ning, and Y. Li, "Robust model predictive control with simplified repetitive control for electrical machine drives," *IEEE Trans. Power Electron.*, vol. 34, no. 5, pp. 4524–4535, May 2019.

[26] A. Mora, Á. Orellana, J. Juliet, and R. Cárdenas, "Model predictive torque control for torque ripple compensation in variable-speed PMSMs," *IEEE Trans. Ind. Electron.*, vol. 63, no. 7, pp. 4584–4592, Jul. 2016.

[27] Q. Fei, Y. Deng, H. Li, J. Liu, and M. Shao, "Speed ripple minimization of permanent magnet synchronous motor based on model predictive and iterative learning controls," *IEEE Access*, vol. 7, pp. 31791–31800, 2019.

[28] J. Wang, D. Huang, S. Fang, Y. Wang, and W. Xu, "Model predictive control for ARC motors using extended state observer and iterative learning methods," *IEEE Trans. Energy Convers.*, vol. 37, no. 3, pp. 2217–2226, Sep. 2022.

[29] P. F. C. Gonçalves, S. M. A. Cruz, and A. M. S. Mendes, "Disturbance observer based predictive current control of six-phase permanent magnet synchronous machines for the mitigation of steady-state errors and current harmonics," *IEEE Trans. Ind. Electron.*, vol. 69, no. 1, pp. 130–140, Jan. 2022.

[30] A. Bemporad, F. Borrelli, and M. Morari, "Model predictive control based on linear programming—The explicit solution," *IEEE Trans. Autom. Control*, vol. 47, no. 12, pp. 1974–1985, Dec. 2002.

[31] S. Bolognani, S. Bolognani, L. Peretti, and M. Zigliotto, "Design and implementation of model predictive control for electrical motor drives," *IEEE Trans. Ind. Electron.*, vol. 56, no. 6, pp. 1925–1936, Jun. 2009.

[32] Z. Mynar, L. Vesely, and P. Vaclavek, "PMSM model predictive control with field-weakening implementation," *IEEE Trans. Ind. Electron.*, vol. 63, no. 8, pp. 5156–5166, Aug. 2016.

[33] C. Jia, X. Wang, Y. Liang, and K. Zhou, "Robust current controller for IPMSM drives based on explicit model predictive control with online disturbance observer," *IEEE Access*, vol. 7, pp. 45898–45910, 2019.

[34] M. Herceg, M. Kvasnica, C. N. Jones, and M. Morari, "Multi-parametric toolbox 3.0," in *Proc. Eur. Control Conf. (ECC)*, Jul. 2013, pp. 502–510.

[35] P. Tøndel, T. A. Johansen, and A. Bemporad, "Evaluation of piecewise affine control via binary search tree," *Automatica*, vol. 39, no. 5, pp. 945–950, May 2003.
[36] X. Chen, J. Wang, B. Sen, P. Lazari, and T. Sun, "A high-fidelity and computationally efficient model for interior permanent-magnet machines considering the magnetic saturation, spatial harmonics, and iron loss effect," *IEEE Trans. Ind. Electron.*, vol. 62, no. 7, pp. 4044–4055, Jul. 2015.
[37] A. S. Yamashita, P. M. Alexandre, A. C. Zanin, and D. Odloak, "Reference trajectory tuning of model predictive control," *Control Eng. Pract.*, vol. 50, pp. 1–11, May 2016.
[38] A. Dorishenko, "Problems of modelling proportional–integral–derivative controller in automated control systems," in *Proc. MATEC Web Conf.*, vol. 112, 2017, p. 5013.
[39] J. A. E. Andersson, J. Gillis, G. Horn, J. B. Rawlings, and M. Diehl, "CasADi: A software framework for nonlinear optimization and optimal control," *Math. Program. Comput.*, vol. 11, no. 1, pp. 1–36, Jul. 2018.
[40] F. Janabi-Sharifi, V. Hayward, and C.-S. J. Chen, "Discrete-time adaptive windowing for velocity estimation," *IEEE Trans. Control Syst. Technol.*, vol. 8, no. 6, pp. 1003–1009, Nov. 2000.

TY TRUNG NGUYEN received the B.S. degree in automatic control engineering from the Hanoi University of Science and Technology, Hanoi City, Vietnam, in 2018. He is currently pursuing the Ph.D. degree in electrical and computer engineering with the School of Information and Communication Engineering, Sungkyunkwan University, Suwon, South Korea. His research interests include motion control, robotics, and embedded systems.

TON HOANG NGUYEN received the B.S. degree in mechatronics engineering from the Ho Chi Minh City University of Technology, Ho Chi Minh City, Vietnam, in 2016, and the Ph.D. degree in electrical and computer engineering from Sungkyunkwan University, Suwon, South Korea, in 2022.

He is currently a Postdoctoral Researcher with the College of Information and Computer Engineering, Sungkyunkwan University. His research interests include signal processing, motion control, robotics, and embedded systems.

JAE WOOK JEON (Senior Member, IEEE) received the B.S. and M.S. degrees in electronics engineering from Seoul National University, Seoul, South Korea, in 1984 and 1986, respectively, and the Ph.D. degree in electrical engineering from Purdue University, West Lafayette, IN, USA, in 1990.

From 1990 to 1994, he was a Senior Researcher with Samsung Electronics, Suwon, South Korea. Since 1994, he has been an Assistant Professor with the School of Electrical and Computer Engineering, Sungkyunkwan University, Suwon, where he is currently a Professor with the School of Information and Communication Engineering. His research interests include robotics, embedded systems, and factory automation.